Molecular Drivers of Self-Assembly in RNA-Loaded lipid nanoparticles Revealed by Coarse-Grained simulations

International Journal of Pharmaceutics 688 (2026) 126449

Contents lists available at ScienceDirect

International Journal of Pharmaceutics

journal homepage: www.elsevier.com/locate/ijpharm

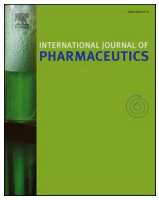

Molecular Drivers of Self-Assembly in RNA-Loaded lipid nanoparticles Revealed by Coarse-Grained simulations

Vincenzo Massotti, Antonio Buffo, Roberto Pisano *

Department of Applied Science and Technology, Politecnico di Torino, 24 corso Duca degli Abruzzi, IT-10129 Torino, Italy

ARTICLE INFO

Keywords:
mRNA pharmaceuticals
Lipid Nanoparticles
Self-Assembly
Molecular Dynamics
Rational Design

ABSTRACT

The development of lipid nanoparticles (LNPs) has revolutionised RNA-based biopharmaceuticals, enabling efficient delivery of mRNA for therapeutic applications. LNPs consist of an ionisable lipid, a neutral phospholipid, cholesterol, and a PEG-ylated lipid (PL). The mixing of an aqueous solution containing mRNA with an ethanol solution containing the lipids leads to the spontaneous formation of mRNA-LNP complexes. However, the mechanisms underlying this process and the behaviour of each component under variable conditions remain partially unclear. Coarse-grained molecular dynamics was here employed to simulate the formation of RNA-loaded LNPs under various conditions, with a specific focus on ethanol. Following exposure to a polar solvent, non-polar forces prevailed, and lipids formed spherical aggregates. Due to Coulombic and hydrophilic interactions, aggregates settled on mRNA surface until they completely cover it. Finally, lipids rearranged depending on their affinity with the surrounding environment. The variation in the ethanol content did not affect the behaviour of lipids, except for the PL: when ethanol was added, the PL tended to migrate toward the inner region of the LNPs. The decrease in PLs on the external surface of LNPs could decrease their ability to regulate particle aggregation, leading to the formation of larger particles at higher ethanol content. Furthermore, higher ethanol fractions resulted in larger, less ordered nanoparticles. Together, these two phenomena could explain the experimental evidence of larger particle produced at higher ethanol content. These findings provide a detailed molecular understanding of LNP self-assembly, offering pivotal insights for designing more stable lipidic carriers for RNA encapsulation.

1. Introduction

Interest in mRNA-based pharmaceuticals has notably increased in recent years. The mRNA therapeutics market was valued at approximately USD 39 billion in 2022 and is projected to exceed USD 100 billion by 2030, with an estimated CAGR above 13 % over the next decade (market research future, 2025). This growth is largely attributed to the rapid deployment of mRNA vaccines during the COVID-19 pandemic, as well as their potential benefits in oncology, rare diseases, and protein replacement therapies (Kim et al., 2021; Pardi et al., 2018; Verbeke et al., 2019). The active pharmaceutical ingredient (API) is a mRNA fragment that is introduced inside the human cells and induces the synthesis of a specific protein. In the treatment of infectious diseases, mRNA stimulates the production of the antibodies necessary for the recognition of the pathogen by the immune system. In the case of oncological or genetic ones, it regulates the synthesis of the growth factor or the protein responsible for the disease.

Despite the several advantages of mRNA pharmaceuticals, this technology has two major drawbacks. mRNA is an anionic macromolecule that very unlikely passes through the non-polar cell membrane. In addition to that, the stability of mRNA is reduced *in vivo* by the presence of RNases, enzymes that decompose the genetic material present in the extracellular space, but also *in vitro* by several mechanisms of physical and chemical degradation (Schoenmaker et al., 2021). Different carriers have been developed over the years to overcome these issues. Among them, lipid nanoparticles (LNPs) seem to be the most effective and safe delivery system for gene therapy (Gote et al., 2023). Their lipidic nature mimics the structure of the cell membrane, facilitating the internalisation of mRNA in the target cells and protecting it from the external environment. LNPs for mRNA delivery are made up of four lipidic species: an ionisable lipid (IL), a neutral lipid (NL), cholesterol, and a PEG-ylated lipid (PL).

ILs are specifically designed for both encapsulation and endosomal release of mRNA into target cells. Their polar head acquires a positive

* Corresponding author.
E-mail address: roberto.pisano@polito.it (R. Pisano).

https://doi.org/10.1016/j.ijpharm.2025.126449
Received 23 September 2025; Received in revised form 28 November 2025; Accepted 29 November 2025
Available online 1 December 2025

charge when exposed to an acidic environment. This feature promotes the encapsulation of mRNA by synthesising the particles at acidic pH. After the synthesis, the neutral charge is restored by bringing back the solution to the physiological pH necessary for storage and administration. ILs are characterised by branched or unsaturated tails that increase the hindrance of the tails compared to that of the head. This feature promotes the formation of inverted micellar structures instead of a lipid bilayer, a conformation that enhances the encapsulation of mRNA (Gruner et al., 1985; Israelachvili, 2011).

On the contrary, NLs have two saturated and linear tails that enhance the formation of a double layer. This feature, in addition to their high transition temperature, makes them suitable for the stabilisation of LNPs. Cholesterol is a fundamental component for the stability of LNPs and their interaction with cell membranes. It fills the gap between the non-polar tails of lipids and modulates their fluidity. A high cholesterol content makes the structure more rigid and reduces the possibility of mRNA leakage during storage and in the bloodstream (Briuglia et al., 2015). Finally, the PLs consist of non-polar tails that integrate on the surface of the LNPs and a long chain of about 45 PEG residues exposed to the external environment. The resulting steric hindrance regulates the size of the nanoparticles and prevents their aggregation during storage and in the bloodstream (Eygeris et al., 2022; Hald Albertsen et al., 2022).

LNPs can be prepared using different techniques, such as emulsion methods, bulk nanoprecipitation, bulk extrusion, and microfluidics (Osouli-Bostanabad et al., 2022; Xu et al., 2022). The latest method enables the synthesis of nanoparticles of controlled size, low polydispersity index and high encapsulation efficiency, showing a high reproducibility and potential for scale-up (Shepherd et al., 2021). RNA and the mixture of lipids are fed to the two opposite ends of the microfluidic device: the former in an aqueous solution at acidic pH and the latter in an ethanol solution. During mixing, the intermolecular forces acting between mRNA and lipids lead to the spontaneous formation of lipid nanoparticles around the mRNA molecules. These nanoparticles generally have a spherical shape characterised by an electron-dense core (Ripoll et al., 2022; Roces et al., 2020). In addition to the spherical shape, some LNPs exhibit large water compartments called “blebs”, usually the result of the dissociation of NLs from the LNP surface. In this configuration, mRNA can be complexed in the lipidic phase or dissolved into the water pools (Brader et al., 2021).

The properties of LNPs and their interactions with the cellular membranes are strictly related to the arrangement of lipids in the nanoparticles. Therefore, a precise understanding of the structure of mRNA-LNPs is crucial for the development of mRNA drugs. In this context, nuclear magnetic resonance spectroscopy (NMR), small-angle X-ray (SAXS), and small-angle neutron scattering (SANS) have been employed to investigate the internal structure of LNPs. These studies have shown that mRNA, when complexed in the lipidic phase, is in disordered cylindrical water compartments with lipids arranged in an inverse hexagonal phase (Arteta et al., 2018). The core of the nanoparticles can be covered by a lipid monolayer, bilayer, or no layer at all (Eygeris et al., 2020; Szebeni et al., 2023). According to Viger-Gravel et al. (Viger-Gravel et al., 2018), the core of these particles is mainly formed by mRNA, ILs, and cholesterol, while the NLs and the PLs are situated on the surface of the particles. In a similar study, Wang et al. (Wang et al., 2023) reported that about 60 % of the ILs are present on the LNPs surface, while small amounts of PLs can be present inside the particle.

Besides experiments, coarse-grained molecular dynamics (CG-MD) simulations have proven to be a valuable tool for investigating the internal organization of LNPs. Coarse graining is a procedure that lowers the computational cost of an MD simulation by grouping atoms in a single particle called “bead”. It reduces the degrees of freedom of the system, and therefore the level of details, but makes it possible to investigate phenomena occurring over wider spatial and temporal scales than a standard MD simulation. The most suitable force field is the MARTINI force field (Souza et al., 2021), specifically tuned for biomolecular simulations and widely used to study lipidic membranes (Kjølbye, 2024). In its latest version, a bead represents 2 to 4 non-hydrogen atoms, providing a good balance between accuracy and computational cost. MD has been widely used to investigate the morphology and the internal organisation of mRNA-loaded LNPs (Gao et al., 2022; Garaizar et al., 2024; Grzetic et al., 2024; Hardianto et al., 2023; Leung et al., 2012; Paloncýová et al., 2025, 2023, 2021; Rissanou et al., 2020; Rozmanov et al., 2014; Trollmann and Böckmann, 2022; Wang et al., 2025; Zhang et al., 2024). Leung et al. (Leung et al., 2012) showed that LNPs exhibit an electron dense core, with siRNA located in disordered water compartments. In this work, LNPs were built starting from small boxes filled with cholesterol, ILs, NLs and siRNA at low hydration levels. These pre-equilibrated boxes were used as building blocks and replicated in all three directions to obtain a larger particle. The external surface was then coated with PLs and re-solvated. Trollmann et al. (Trollmann and Böckmann, 2022) used a similar procedure to investigate the effect of the pH on the retention of mRNA. LNPs were formed using two different building blocks. The first one composed by mRNA, ionisable lipid and cholesterol was used as a building block for the core of the nanoparticle. The second block was mainly made up of cholesterol and neutral lipids and was used as a building block for the shell on LNPs. The mRNA-loaded LNP was then formed by duplicating the core blocks and covering them with a series of shell ones and with PLs. These approaches are strongly guided by experimental results, as the species forming the core and the shell were artificially placed in the expected position.

Paloncyova et al. (Paloncýová et al., 2023) used a different approach, generating small boxes where individual lipids were randomly dissolved. These boxes were then enlarged and filled with water to induce the formation of the nanoparticles. In accordance with previous studies, this work reports a loss of mRNA upon exposure to a neutral pH. Wang et al. (Wang et al., 2025) simulated particles with a diameter of around 80 nm, providing insights into the morphology of LNPs at their actual size. Under these conditions, the shift from acidic to neutral pH did not lead to the release of encapsulated mRNA into the external environment. Despite offering valuable information on lipid organisation within the particle, the LNPs in these studies are generated from preassembled components or under conditions that strongly drive their assembly. Therefore, these studies do not describe the dynamics of self-assembly in conditions similar to experimental ones. Recently, Grzetic et al. (Grzetic et al., 2024) developed a CG force field that maps 10 heavy atoms in a single bead, significantly extending the length scales accessible in molecular simulations. By enabling the simulation of more diluted systems, the results of this study highlight the various steps leading to the formation of LNPs. However, this approach leads to a loss of resolution at the atomistic scale, and the interactions between the different species cannot be described in detail. Furthermore, the role of ethanol in influencing the assembly and morphology of LNPs remains unclear, as current studies focus on lipid and mRNA assembling in pure water.

This work aims to cover these gaps, providing a more realistic description of the self-assembling process of mRNA-LNP complexes. Differently from previous studies, where LNPs formation was highly forced, CG-MD simulations start from a condition in which the different species are randomly dispersed in the co-solvent mixture and spontaneously interact to form the final nanoparticles. The simulation of more diluted systems allowed us to capture the different steps of the self-assembling process, reducing the bias induced by the initial conformation of lipids and mRNA. Furthermore, the composition of the co-solvent mixture was here varied to assess the effect of different process parameters on the mechanism of self-assembling, the properties of the nanoparticles and the interactions of RNA with the lipidic formulation. This aspect has been overlooked in previous works, which often neglect the presence of ethanol in the system. As the results of this study provide a complete and more representative description of the self-assembling process, they could be extremely helpful in the design of LNPs. The

development of an *in vitro* platform could drive the design of new lipidic species specifically engineered to optimise both the encapsulation of mRNA and its delivery to the site of action.

2. Methods

mRNA and the mixture of lipids were randomly placed in a cubic simulation box. Short RNA chains of 10 (Small-RNA, S), 50 (Medium-RNA, M), and 200 (Large-RNA, L) uracil residues were chosen as template molecules for mRNA. According to the standard formulation of RNA vaccines (Schoenmaker et al., 2021), the N/P ratio (molar ratio between ionisable lipids and RNA residues) was set to 6, and the lipid molar ratio between IL:Chol:NL:PL to 50:38.5:10:1.5. ALC-0315, Distearoylphosphatidylcholine (DSPC) and ALC-0159 were used as IL, NL, and PL, respectively. The excess of the ionizable lipids generate a net positive charge, which was neutralized by adding Cl^- ions in the solution. Using the composition of the different flows in a microfluidic mixer as a reference, lipids and mRNA were dissolved in solvents of different compositions. Starting from pure water, the molar fraction of ethanol was varied to simulate different Flow Rate Ratios (FRRs) in a microfluidic device. Temperature and pressure were maintained constant at 310 K and 1 bar, respectively. A summary of the simulated operating conditions is reported in Table 1.

3. Simulations Setup

Simulations were performed using GROMACS 2022.3 (Abraham et al., 2015) and the third version of the Martini force field (Souza et al., 2021). Topologies of poly-U RNA fragments, ALC-0315 and ALC-0159 were obtained by a previous work by Paloncyova et al. (Paloncýová et al., 2023), while that of cholesterol from its latest release for Martini 3 force field (Borges-Araújo et al., 2023). A schematic of the present species and their CG structures is reported in Fig. 1.

The systems were equilibrated in the NPT ensemble for 500 ns with a time step of 5 fs. The preliminary simulations with mRNA of variable size aimed to capture the dynamics of the early steps of self-assembly and were carried out for 3 μs with a time step of 10 fs. To investigate the effect of ethanol, simulations with different ethanol content were carried out for 10 μs (time step = 10 fs), with three replicas per system. The temperature and the pressure were controlled with the v-rescale thermostat (Bussi et al., 2007) ($\tau_T = 4$ fs) and the c-rescale barostat (Bernetti and Bussi, 2020) ($\tau_P = 20$ fs), respectively. The PME (Darden et al., 1993) algorithm was used to manage electrostatic and Van der Waals interactions with a cut-off of 1.3 nm. The final properties of mRNA-LNPs complexes were evaluated averaging them over the last μs of the production run. The software Visual Molecular Dynamics (VMD) (Humphrey et al., 1996) was used to generate snapshots from the trajectory file.

Radial distribution functions (RDFs) were computed using RNA beads as reference, with the bead of lipids and ions selected as the groups for which the distribution functions were calculated.

The affinity between the different species was evaluated by computing the number of contacts (NCs) between them. All species, except mRNA, were broken into heads and tails, the hydrophilic (H) and the hydrophobic (T) ends of each species, respectively. The H-group of each species included the charged, polar and intermediately polar beads, i.e. the blue, orange and yellow beads depicted in Fig. 1. Conversely, T-groups comprised the non-polar beads, identified as green beads in Fig. 1. Two groups were considered in contact when their distance decreased below 0.6 nm. The NCs of group i with each group j was computed and expressed as the percentage of the total NCs (%NC) of group i, according to the following equation:

$$\%NC_{i,j} = \frac{NC_{i,j}}{\Sigma_j NC_{i,j}}\%. \quad (1)$$

The solvent accessible surface area (SASA) was computed using a probe with a radius equal to 0.191 nm, corresponding to a tiny bead in the latest version of Martini force field. The same procedure has been employed to estimate the volume enclosed by the SASA, corresponding to the volume not accessible by the solvent. The size of LNPs was then estimated as the diameter of a sphere that has a volume equal to the excluded volume.

4. Results and Discussion

4.1. Simulation of the self-assembly mechanism driving mRNA encapsulation

To replicate the mixing of the two solutions within the microfluidic device, mRNA and lipids were randomly placed in the simulation box. The system was then solvated with a mixture of water and ethanol to reproduce an FRR equal to 3:1, known as the optimal value for this parameter (Roces et al., 2020).

Fig. 2 shows snapshots extracted from the trajectory of solutes during the simulation. At the beginning of the simulation, lipids and RNA were randomly distributed throughout the simulation box (Fig. 2a). When exposed to a polar solvent like the mixture of water and ethanol, lipids tended to form small aggregates to minimise contact with solvent molecules (Fig. 2b). The lipidic tails and cholesterol tended to move into the core of the aggregates, while the hydrophilic heads were exposed at the interface with water. These aggregates had a random lipidic composition and took on a spherical shape characterised by an inverted micellar arrangement. mRNA started to interact with lipidic clusters due to Coulombic or hydrophilic interactions, forming little complexes where mRNA settled on the surface of the rising nanoparticle. To further reduce the surface exposed to the solvent, lipids continued to aggregate until they formed a single mRNA-LNP complex (Fig. 2c-f). Inside the LNP, mRNA tended to form clusters that should be the result of base pairing between uracil bases of different RNA molecules. Due to the tendency of lipids to form double layers, the final particle deviated from the spherical shape forming empty water pockets.

In this simplified system, mRNA was assimilated to a short fragment made up of 10 residues (Small-RNA). The interactions described here can be extended to the case of an entire mRNA molecule made of thousands of bases, but the self-assembling mechanism could be slightly different. To evaluate whether the self-assembling is affected by the size of the mRNA, RNA fragments were substituted by bigger ones. The total number of RNA residues was kept constant at 200, replacing small fragments with 4 chains made up of 50 residues (Medium-RNA) and 1 chain made up of 200 ones (Large-RNA). The mechanism of the self-

Table 1
Details on the composition of the simulation boxes.

Simulation	N_{bases}	N_{RNA}	N_{IL}	N_{NL}	N_{chol}	N_{PL}	N_{CL}	N_{water}	N_{EtOH}	Simulation time, μs
S-3:1	200	20	1200	240	924	36	1000	84,932	35,068	3
M−3:1	200	4	1200	240	924	36	1000	84,932	35,068	3
L-3:1	200	1	1200	240	924	36	1000	84,932	35,068	3
S-1:0 x3	100	10	600	120	462	18	500	120,000	0	10
S-3:1 x3	100	10	600	120	462	18	500	84,932	35,068	10
S-1:1 x3	100	10	600	120	462	18	500	53,604	66,396	10

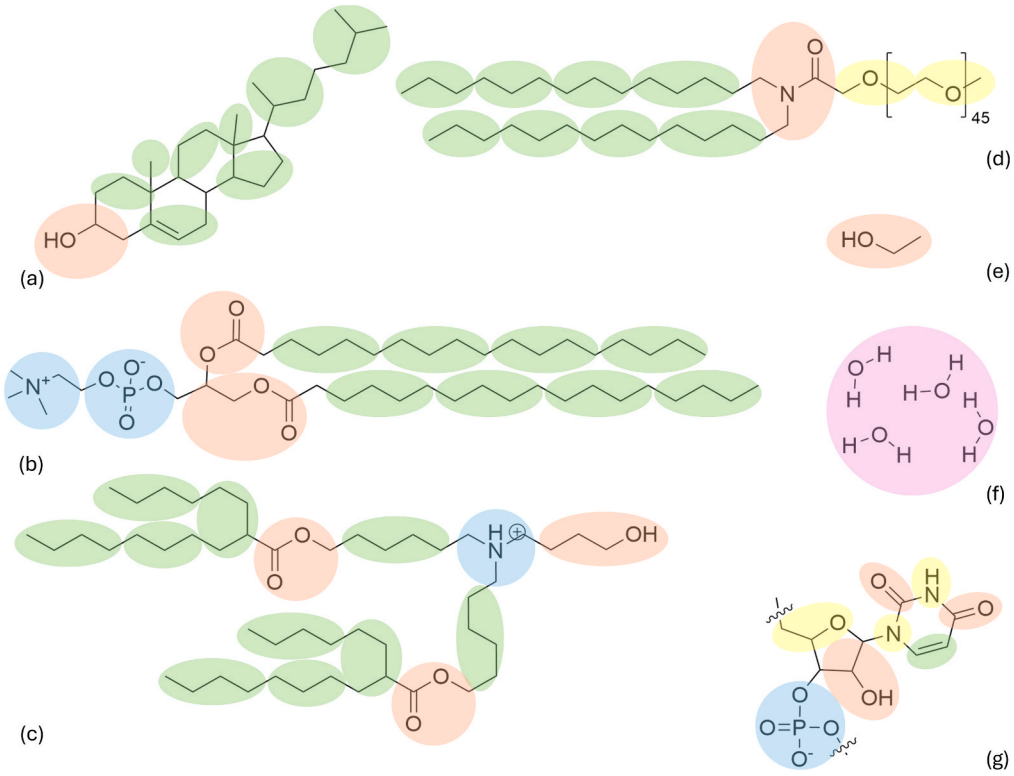

Fig. 1. Schematic of the chemical structure and coarse grain mapping of (a) cholesterol, (b) DSPC, (c) ALC-0315, (d) ALC-0159, (e) ethanol, (f) water and (g) uracil residue. The atoms present in each species were grouped in (green) non-polar, (yellow) intermediately polar, (orange) polar, (blue) charged, and (purple) water beads.

assembling in the new systems is reported in Figs. S1 and S2 in the Supporting Information. It was very similar to the previous case study, with lipids that started to form small clusters that gradually interacted with RNA. Since RNA was bigger, it seemed to accelerate the coalescence of the particles that gradually settled on its surface. At the end of the process, the RNA molecules were entirely encapsulated in the LNP and isolated from the external environment.

The mechanism described by CG-MD simulations can be outlined in three steps, as reported in Fig. 3. The process was driven by the aggregation of lipids, and the interactions with mRNA began at a later stage. For this reason, the following description would remain valid even changing the lipid species or their molar ratios. At first, the organic and the aqueous phase were segregated, with lipids and mRNA completely dissolved in ethanol and water, respectively (Fig. 3a). When the two streams started to mix, lipids started to randomly aggregate due to their insolubility in water (Fig. 3b). Due to Coulombic and hydrophilic interactions, lipidic clusters interacted with mRNA and started to cover its surface. To further reduce the interface with the solvent, lipidic clusters tended to coalesce to form bigger particles (Fig. 3c). In the final step of the process, lipids tended to rearrange and consolidate their structure depending on their affinity with the external environment (Fig. 3d).

4.2. Lipid arrangement and morphology of the final assembly

At the end of the simulations, lipids and RNA formed a unique cluster with mRNA encapsulated in the core of the LNP. As an example, Fig. 4 reports the clusters extracted from the last frame of the simulation of the Large-RNA. Although the initial clusters had a random lipidic composition, species tended to occupy specific positions in the final configuration. IL is the most abundant component in the formulation, and it was distributed throughout the nanoparticle. NLs and PLs tended to cover the external surface of the nanoparticle due to their higher hydrophilicity. Cholesterol, as expected, was complexed into the lipidic tails because of its strong hydrophobicity. A cross-section of the nanoparticles is reported in Fig. 4b to observe the internal organization of the mRNA-LNP complex. mRNA could be contained in inverted micellar or disordered cylindrical cavities, as confirmed by previous experiments (Arteta et al., 2018; Brader et al., 2021; Eygeris et al., 2020; Szebeni et al., 2023) and simulations (Leung et al., 2012; Paloncýová et al., 2023; Wang et al., 2025). The cross section highlights the presence of empty water pockets, detectable as areas where the density of the lipidic matrix is lower.

In addition to the visual inspection, radial distribution functions (RDFs) were computed to investigate the arrangement of lipids around mRNA. RDFs of the four lipidic species and the Cl^- ions computed from the surface of Small, Medium, and Large-RNA are reported in Fig. 5. ILs presented a single peak in their distribution, indicating that they were distributed throughout the particle. In all three cases, the peak slightly shifted to the left because of their affinity with the nucleic acid. Cholesterol showed a similar behaviour, with a single peak located in the middle of the lipidic phase.

On the contrary, NLs and PLs showed a single or a double peak in the inner and/or in the outer part of the particle. These species were not present in the bulk of the lipidic phase but tended to dispose at the interface with the solvent. NLs seemed to be always present in both interfaces, with peaks of different heights that may be the result of the stochastic nature of the self-assembling. On the other side, PLs can or not remain trapped in the inner part of the particle. Both species showed a high hydrophilicity compared to the other lipids, a property that caused their migration to the interfaces with solvents. In the case of PLs, the steric hindrance of the long PEG-ylated chains enhanced its migration to the external surface of LNPs. To balance the positive charge of the ILs, Cl^- ions tended to accumulate in the inner side of LNPs, and they showed a lower peak on the external surface of the nanoparticles.

In the simulations of these diluted systems, lipids and mRNA gradually interacted to form the final nanoparticle, highlighting the different

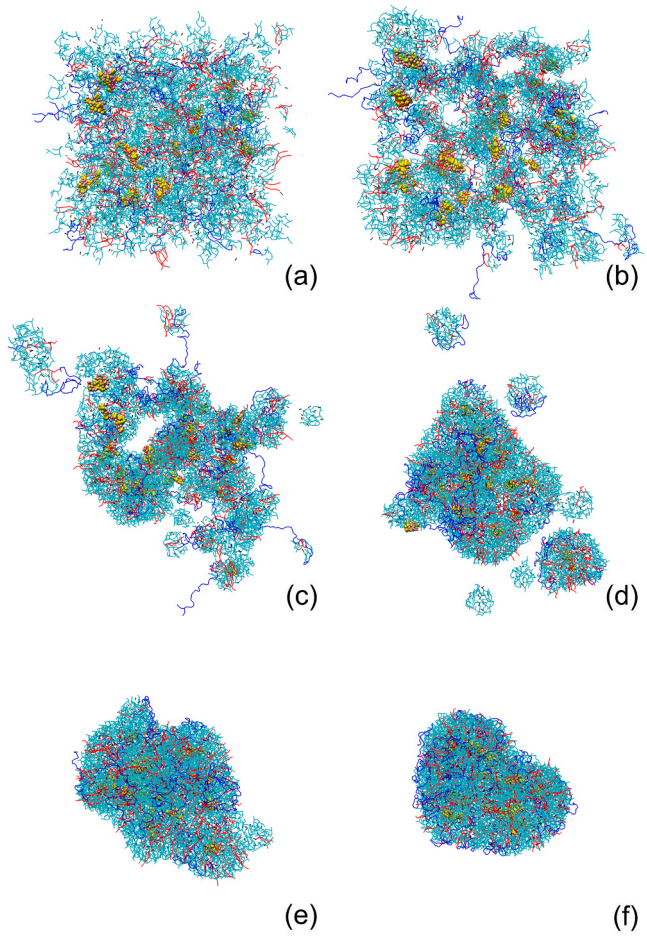

Fig. 2. Snapshots extracted from the trajectory of Small-RNA and lipids at 0 (a), 1 (b), 5 (c), 50 (d), 300 (e),1000 (f) ns. At the beginning of the simulation, the lipidic mixture containing the ionisable (cyan), neutral (red), PEG-ylated lipids (blue) and cholesterol (black) was randomly distributed throughout the simulation box Then, lipids started to form small clusters of random composition that gradually fused in a single one encapsulating mRNA.

steps that led to its formation. The molecules were free to interact, and spontaneously arranged themselves in positions where they were more stable, not affected by the initial conformation. These results were consistent with previous experimental studies (Arteta et al., 2018; Ueda et al., 2023; Viger-Gravel et al., 2018), supporting the validity of the mechanistic description of the self-assembly provided in the previous section. mRNA is contained in disordered cylindrical channels with lipids in an inverted hexagonal arrangement. ILs strongly interact with RNA but are also present on the surface of LNPs. NLs and PLs tend to cover the external surface of the particles and, in traces, can be found at the interface with the water pools containing RNA. Finally, cholesterol fills the gaps between the hydrophobic tails of the other lipids.

4.3. RNA affinity with the lipidic formulation

The phenomenon of self-assembling is driven by the molecular interactions between the species present in the system. A precise understanding of these interactions could be extremely helpful in the design of future and more performing lipidic species. To improve the statistical reliability of the number of contacts between the species in the system, simulations were repeated in triplicate. Table 2 reports the %NC of species *i* (rows) with all other species *j* (columns), averaged over the three replicas of the system with a FRR equal to 3:1. The analysis of the %NC underlines that non-polar species strictly interacted with one another, forming the hydrophobic core of the particle. Approximatively 52–66 % of contacts of the lipidic tails took place with other lipidic tails, while around 17–22 % occurred with cholesterol. Focusing on cholesterol, 54 % of its contacts occurred with molecules of the same species. This behaviour might be due to the scarce solubility of cholesterol in the unsaturated lipidic tails of ILs. Consequently, cholesterol tended to cluster and can arrange in a crystalline form (Szebeni et al., 2023).

On the other side, the hydrophilic ends tended to interact with the solvent, with which they establish 43–65 % of their contacts. Each of the three species preferentially interacted with water, the most abundant co-solvent, and behaved differently based on their hydrophilicity. For the ILs, the difference in the %NC with water and ethanol was approximately 33 %, while for NLs and PLs this value increased to around 48 % and 57 %, respectively, due to their higher affinity with water. Being exposed to the interface, a small number of contacts occurred between the heads of different species, including cholesterol with its small hydroxyl group. Despite the low affinity between polar and non-polar

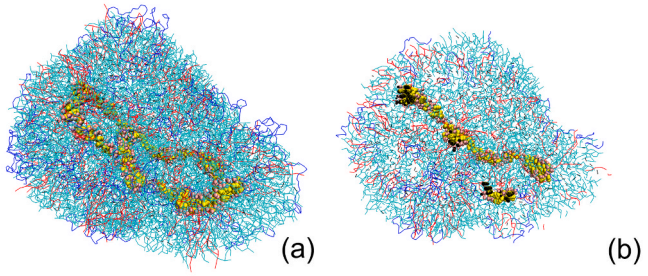

Fig. 4. (a) mRNA-LNP complex and (b) its cross-section extracted from the last frame of the simulations of Large-RNA. mRNA is located in water pockets of disordered cylindrical shape with lipids in an inverted hexagonal arrangement. ILs (cyan) and cholesterol (black) form the bulk of the lipidic phase, while NLs (red) and PLs (blue) cover the external surface of the particle.

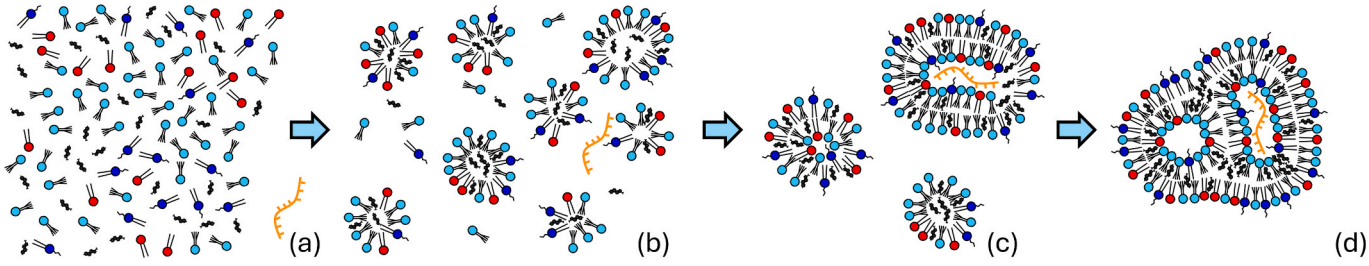

Fig. 3. Schematic of the self-assembling of mRNA-LNPs complexes. (a) Ionisable (cyan), neutral (red), PEG-ylated lipids (blue) and cholesterol (black) are dissolved in the organic phase, while mRNA (orange) is dissolved in water. (b) At the beginning of the process, non-polar forces prevail, and lipids tend to aggregate randomly. Some lipids clusters can settle on mRNA surface starting the encapsulation process. (c) The aggregation of the lipidic clusters continue, completely covering the mRNA surface and reducing their interface with water. (d) According to their affinity with the external environment, lipids rearrange and consolidate the structure of the final particle.

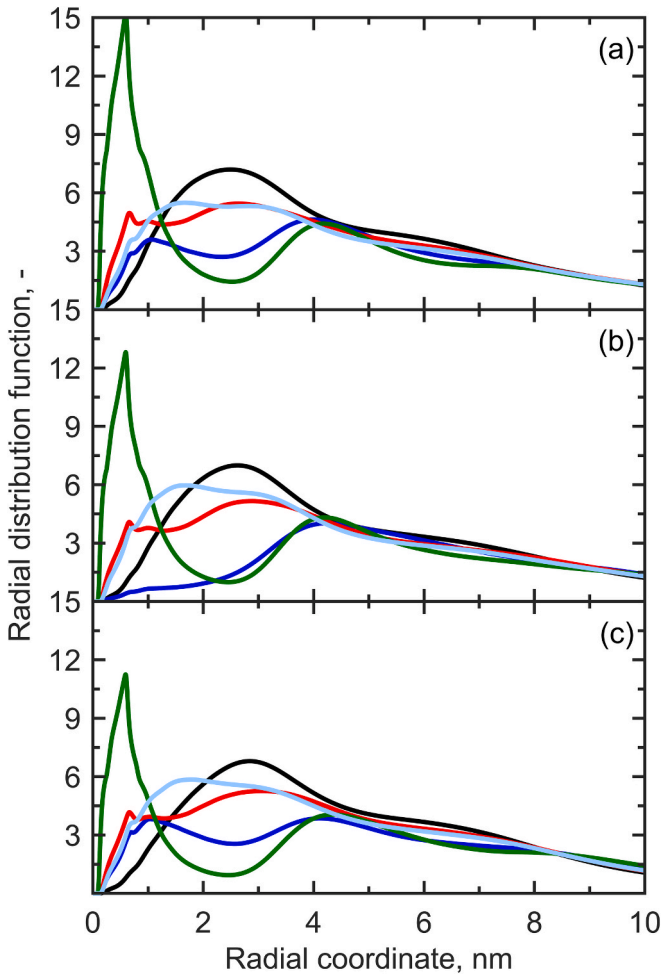

Fig. 5. Radial distribution functions of lipids and Cl^- ions around Small (a), Medium (b), and Large RNA (c). Peaks corresponding to ILs (cyan curve), and cholesterol (black curve) are localised in the middle of the lipidic phase, with ILs slightly shifted on the left because of their affinity with RNA. NLs (red curve) and PLs (blue curve) show single or double peaks at the inner or the outer interface with solvents due to their hydrophilicity. Cl^- ions (green curve) presented two peaks, as the ions tended to accumulate in regions with higher positive charge.

groups, they exhibited a non-negligible %NC. This result may be due to the presence of ester linkers in the tails of both NL and IL. They affinity with external polar groups can facilitate closer contact between non-compatible beads and increase their number of contacts. Furthermore, the increase in the %NC may be caused by interactions of the two portions of the same molecule. Since both lipids and mRNA adopted a stretched configuration, the number of self-contacts was expected to be negligible compared to contacts with other species.

Passing to RNA, it mainly interacted with other RNA molecules, highlighting the tendency of RNA to form clusters as proposed in a previous study (Szebeni et al., 2023) and confirmed by molecular simulations (Paloncýová et al., 2023). Its interactions with ILs were approximatively five times those with NLs, reflecting the molar ratio between the two lipids in the formulation. Despite the neutral charge, the chemistry of the polar head of NLs is similar to that of ILs, and its polarity made its interaction with RNA non-negligible.

To further investigate the interactions involving RNA, the %NC were re-computed for the RNA backbone (BB) and side chain (SC). The %NC between positive (+), negative (−), ester (−EL) or hydroxyl groups (–OH) with BB or SC is expressed as a fraction of the total number of contacts of that portion of lipid with RNA. Table 3 reports the %NC of the two fractions of RNA with each other and with the polar groups of ILs and NLs. Despite the Coulombic attraction between the phosphate group in the BB and the positive head of ILs, it similarly interacted with the SC. These interactions could arise from the excess of ILs compared to RNA, as the N/P ratio was set to 6. ILs that did not interact with BB seemed to establish an alternative mechanism of interaction with RNA, which may persist even when the neutrality of the system is re-established. Moreover, the hydroxyl groups showed a good affinity with the SC as if they were able to form hydrogen bonds typical of base pairing (Cornebise et al., 2022; Szebeni et al., 2023). The slight polarity of the ester linker caused this portion of the lipid to predominantly interact with the BB. These interactions with the RNA-SC could be the reason why mRNA and ILs continue to interact even when ILs are in their neutral form. However, due to the low resolution of the CG at the atomistic level, all-atoms simulations could provide a better understanding of the nature of this phenomenon. Future work could focus on these interactions, accelerating the self-assembly process through coarse-grained simulations and analysing them by back-mapping the final structure to its atomistic resolution. On the contrary, because of their neutral head, NLs preferentially interacted with the SC, confirming the strong affinity of the heads of lipids with this portion of RNA. Finally, the %NC between the two portions of RNA shows that RNA tended to cluster by establishing hydrogen bonds between the nitrogen bases present in the SC.

Table 3
Percentage of the total number of contacts between RNA backbone (BB) and sidechain (SC) and (+) positive, (−) negative, (–OH) hydroxyl, and (−EL) ester linker of ILs and NLs. The results were averaged over the three replicas of the system.

	BB	SC
IL+	46.83 %	53.17 %
IL-OH	40.44 %	59.56 %
IL-EL	57.39 %	42.61 %
NL+	30.55 %	69.45 %
NL-	37.33 %	62.67 %
NL-EL	50.29 %	49.71 %
BB	42.28 %	57.72 %
SC	25.33 %	74.67 %

Table 2
Percentage of the total number of contacts with a FRR equal to 3:1 averaged over the three replicas. Hydrophilic groups are denoted with the letter H, while hydrophobic ones are denoted with the letter T.

	IL-H	IL-T	NL-H	NL-T	CHOL-H	CHOL-T	PL-H	PL-T	RNA	CL	W	ETOH
IL-H	9.5 %	25.7 %	1.5 %	1.4 %	2.3 %	6.6 %	2.9 %	0.2 %	4.9 %	2.2 %	37.8 %	5.1 %
IL-T	13.4 %	45.9 %	0.5 %	5.5 %	1.5 %	17.4 %	1.6 %	0.9 %	0.4 %	0.2 %	10.5 %	2.1 %
NL-H	6.1 %	3.9 %	11.7 %	4.4 %	1.6 %	1.9 %	4.1 %	0.1 %	4.0 %	1.0 %	54.9 %	6.5 %
NL-T	4.8 %	37.0 %	3.8 %	24.9 %	1.2 %	22.3 %	0.8 %	1.2 %	0.0 %	0.0 %	3.1 %	0.9 %
CHOL-H	11.8 %	15.0 %	2.1 %	1.8 %	3.2 %	27.4 %	2.2 %	0.2 %	4.2 %	2.4 %	25.5 %	4.2 %
CHOL-T	5.3 %	26.9 %	0.4 %	5.1 %	4.2 %	53.7 %	0.5 %	0.7 %	0.2 %	0.1 %	2.3 %	0.7 %
PL-H	6.3 %	6.7 %	2.2 %	0.5 %	0.9 %	1.2 %	14.7 %	0.4 %	0.3 %	1.9 %	60.9 %	4.0 %
PL-T	4.6 %	39.3 %	0.3 %	8.1 %	0.8 %	21.0 %	4.0 %	18.5 %	0.0 %	0.0 %	2.7 %	0.7 %
RNA	10.3 %	1.7 %	2.0 %	0.0 %	1.7 %	0.5 %	0.3 %	0.0 %	68.6 %	4.3 %	9.2 %	1.4 %

4.4. Effect of ethanol

The FRR (aqueous/organic flow rate) is one of the two processing parameters that influence the size and the polydispersity of the LNPs, with both decreasing as FRR increases (Ripoll et al., 2022; Roces et al., 2020). To evaluate the molecular phenomena that lead to these results, lipids and RNA were dissolved in different solvents with an increasing quantity of ethanol. Keeping the number of solvent molecules constant, some water beads were replaced with ethanol ones. The simulations were repeated with a molar fraction of ethanol equal to 0, 0.09, and 0.24, corresponding to an FFR of 1:0, 3:1, and 1:1, respectively. To improve the statistical reliability of the dataset, simulations were repeated in triplicate.

Fig. 6 reports the RDFs of the four lipidic species around mRNA. The distributions of NLs, ILs and cholesterol (Fig. 6a-c) were very similar in the three cases, with a difference in their peaks that may be associated to the different size of ethanol and water bead. The RDFs of cholesterol showed a slight shift toward shorter distances as the water content increased. When particles were exposed to a more polar solvent, i.e. higher concentration of water, lipids were more forced to assemble due to their insolubility. In these conditions, the particle may show a more compact structure, characterised by a core enriched of lipidic species. Conversely, the ethanol content modified the RDFs of PLs, that showed a single or double peak depending on the presence of ethanol. When ethanol was not present in the system (blue curve in Fig. 6d), PLs showed a single peak on the external surface of the LNPs. On the contrary, when ethanol was added to the simulation box PLs showed an additional peak on the inner side of the LNPs. As previously discussed, PLs are more likely to interact with water than ethanol. Therefore, when the number of ethanol beads increased, PLs tended to migrate in a more polar environment as the cavities containing mRNA. The decrease in the PLs exposed on the external surface may decrease their ability to regulate particle aggregation, leading to the formation of larger particles. This result could explain the increase in particle size observed in experimental studies (Ripoll et al., 2022; Roces et al., 2020). These works report that the particle size at a FRR of 1:1 is approximatively twice that measured at a FRR of 3:1.

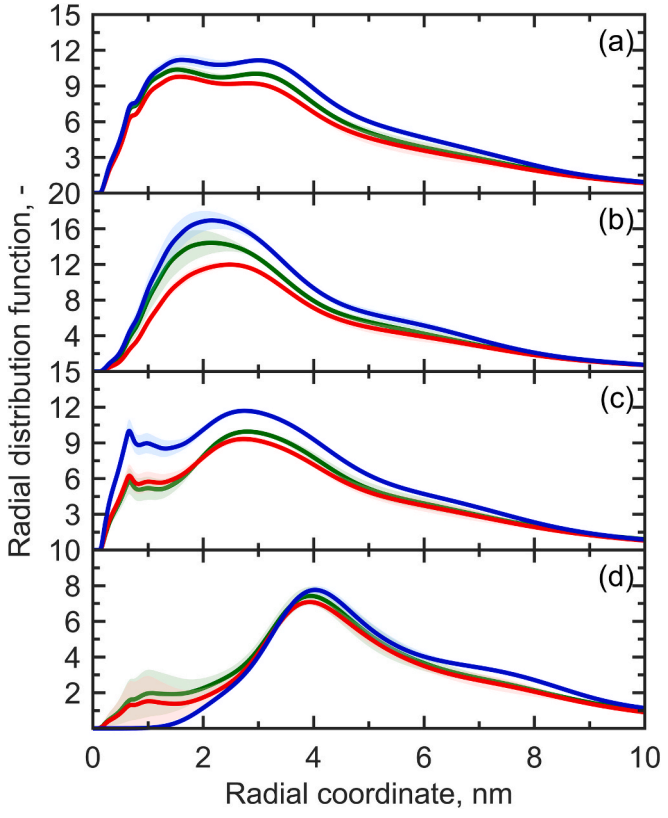

Fig. 6. Radial distribution functions of (a) ILs, (b) cholesterol, (c) NLs and (d) PLs around mRNA in case of FRR equal to 1:0 (blue curve), 3:1 (green curve) and 1:1 (red curve). The solid line represents the average distribution, while the lighter shade the standard deviation observed over the three replicas of each system. ILs, cholesterol and NLs showed a similar behaviour in the different environments. PLs showed remarkable differences, as their peaks in the inner parts of the particles increase with the ethanol content.

Tables 4-6 report the %NC in case of FRR equal to 1:0 and 1:1 averaged over the three replicas of each system. In both, the interactions between the lipidic formulation and mRNA were not affected by the presence of ethanol, showing a similar trend previously observed. The only difference lied in the interaction with the co-solvents, as lipids have a higher affinity with ethanol than with water. For this reason, as the ethanol content increased, they increased their contact with the organic solvent and decreased their contact with water.

To analyse the distribution of the two co-solvents within the LNPs, RDFs of ethanol and water beads around RNA are reported in Fig. 7. In all three cases, the distributions showed a peak in the regions close to the mRNA surface, indicating that mRNA is surrounded by solvent molecules in the cavity of the lipidic phase. After a decrease due to the presence of the lipidic phase, the curves reached their maximum at greater distances, as water and ethanol were most distributed outside the nanoparticle. Differently from water, RDFs of the organic solvent did not decrease to zero when moving from the inner to the outer part of the LNP. This result suggest that ethanol may remain in the non-polar core of the nanoparticle due to its affinity with the lipidic tails. Its presence in the membrane could reduce its compactness, altering the morphology of LNPs. The increase in the ethanol content caused a slight increase in both the RDFs, indicating a higher penetration of both water and ethanol inside the nanoparticles. These results suggested an increase in LNPs permeability due to their solubility in ethanol (Hardianto et al., 2023), which facilitated the migration of water and ethanol into the particle.

To further investigate this effect and to estimate the size of the LNPs, the solvent accessible surface area (SASA) and the particle size were computed as a function of the ethanol molar fraction. As shown in Fig. 8, both SASA and the particle size increased with the molar fraction of ethanol, confirming the behaviour observed in previous experimental studies (Ripoll et al., 2022; Roces et al., 2020). When exposed to an environment characterized by a higher ethanol content, lipids were less forced to assemble due to their higher affinity with ethanol than water. Consequently, they assembled and formed a more disordered and less compact structure characterized by a higher SASA, which increased as the ethanol molar fraction increases. As a result of the disordered and less forced assembly, the particles showed a slight increase in the particle size. This effect is expected to be more significant in real-size particles, which are approximately ten times larger than those examined in this study.

5. Conclusions

In this work, CG-MD was employed to investigate the phenomena that occur during the synthesis of LNPs containing RNA. Starting from a disperse phase, lipids and mRNA were free to interact in a mixture of water and ethanol of variable composition. The results of the simulations showed that the self-assembling of lipids and mRNA was characterised by three different steps. At first, lipids tended to form small aggregates of casual composition to minimize exposure to the solvent. These aggregates gradually settled on the surface of mRNA until they completely covered it, further reducing the contact with the solvent. During the coalescence of these particles, lipids rearranged according to their affinity with the surrounding environment. A spherical shape with a dense core characterised the final LNP. mRNA clusters are dissolved into cylindrical water pools bordered by lipids in an inverted hexagonal arrangement. It mainly interacted with ILs, which demonstrated a high

Table 4
Percentage of the total number of contacts with a FRR equal to 1:0 averaged over the three replicas. Hydrophilic groups are denoted with the letter H, while hydrophobic ones are denoted with the letter T.

	IL-H	IL-T	NL-H	NL-T	CHOL-H	CHOL-T	PL-H	PL-T	RNA	CL	W
IL-H	9.1 %	24.3 %	1.6 %	1.3 %	2.2 %	6.1 %	2.5 %	0.2 %	4.2 %	2.0 %	46.4 %
IL-T	13.3 %	45.3 %	0.5 %	5.4 %	1.5 %	16.7 %	1.5 %	0.9 %	0.4 %	0.2 %	14.3 %
NL-H	6.3 %	3.7 %	10.9 %	4.0 %	1.7 %	1.8 %	3.2 %	0.1 %	5.6 %	0.9 %	61.9 %
NL-T	5.0 %	36.7 %	3.7 %	24.8 %	1.3 %	22.6 %	0.6 %	1.2 %	0.0 %	0.0 %	4.0 %
CHOL-H	11.7 %	14.9 %	2.3 %	1.9 %	3.5 %	27.3 %	1.5 %	0.2 %	4.3 %	2.3 %	30.1 %
CHOL-T	5.3 %	26.4 %	0.4 %	5.2 %	4.3 %	54.3 %	0.3 %	0.7 %	0.2 %	0.1 %	2.8 %
PL-H	5.2 %	5.9 %	1.7 %	0.4 %	0.6 %	0.7 %	12.4 %	0.3 %	0.0 %	1.5 %	71.4 %
PL-T	4.9 %	40.1 %	0.3 %	7.9 %	0.8 %	19.2 %	3.8 %	18.5 %	0.0 %	0.0 %	4.4 %
RNA	9.3 %	1.6 %	3.1 %	0.0 %	1.7 %	0.5 %	0.0 %	0.0 %	68.6 %	3.9 %	11.3 %

Table 5
Percentage of the total number of contacts with a FRR equal to 1:1 averaged over the three replicas. Hydrophilic groups are denoted with the letter H, while hydrophobic ones are denoted with the letter T.

	IL-H	IL-T	NL-H	NL-T	CHOL-H	CHOL-T	PL-H	PL-T	RNA	CL	W	ETOH
IL-H	10.1 %	27.6 %	1.6 %	1.5 %	2.3 %	7.2 %	3.3 %	0.2 %	5.2 %	2.6 %	26.9 %	11.4 %
IL-T	13.5 %	46.9 %	0.5 %	5.6 %	1.5 %	18.1 %	1.7 %	0.9 %	0.4 %	0.2 %	6.4 %	4.4 %
NL-H	6.7 %	4.2 %	13.6 %	5.0 %	1.9 %	2.2 %	4.9 %	0.1 %	5.3 %	1.2 %	40.0 %	14.9 %
NL-T	4.7 %	36.7 %	3.8 %	25.2 %	1.2 %	22.6 %	0.8 %	1.2 %	0.0 %	0.0 %	1.8 %	1.9 %
CHOL-H	11.8 %	15.0 %	2.2 %	1.8 %	2.9 %	28.0 %	2.6 %	0.2 %	3.0 %	2.8 %	19.5 %	10.0 %
CHOL-T	5.3 %	27.2 %	0.4 %	5.2 %	4.1 %	53.2 %	0.5 %	0.7 %	0.1 %	0.1 %	1.6 %	1.5 %
PL-H	7.5 %	7.8 %	2.6 %	0.6 %	1.2 %	1.7 %	18.0 %	0.4 %	0.3 %	2.5 %	47.6 %	9.7 %
PL-T	4.5 %	39.4 %	0.3 %	8.2 %	0.8 %	21.2 %	4.1 %	18.7 %	0.0 %	0.0 %	1.5 %	1.4 %
RNA	10.0 %	1.5 %	2.4 %	0.0 %	1.2 %	0.3 %	0.3 %	0.0 %	69.5 %	4.6 %	7.1 %	3.1 %

Table 6
Percentage of the total number of contacts between RNA backbone (BB) and sidechain (SC) and (+) positive, (−) negative, (–OH) hydroxyl, and (−EL) ester linker of ILs and NLs. The results were averaged over the three replicas of the systems.

	FRR 1:0		FRR 1:1	
	BB	SC	BB	SC
IL+	49.71 %	50.29 %	48.14 %	51.86 %
IL-OH	43.30 %	56.70 %	40.66 %	59.34 %
IL- EL	59.88 %	40.12 %	59.53 %	40.47 %
NL+	27.88 %	72.12 %	29.50 %	70.50 %
NL-	36.30 %	63.70 %	37.28 %	62.72 %
NL- EL	53.92 %	46.08 %	54.51 %	45.49 %
BB	42.20 %	57.80 %	42.33 %	57.67 %
SC	24.55 %	75.45 %	25.12 %	74.88 %

affinity with both BB and SC of the RNA chains. Despite the positive charge of ILs, they were also present on the surface of LNPs, exposing their polar head to the external environment. The external surface of LNPs was rich in NLs and PLs that tended to migrate to the interface with water. This migration was due to the high hydrophilicity of their headgroup, which was accentuated by the steric hindrance of the long PEG-ylated chains in the case of PLs. Finally, cholesterol filled the gap between the non-polar tails due to its strong hydrophobicity and interacted with the polar environment through its hydroxyl group. Increasing the ethanol content in the system, i.e., decreasing the FRR between water and ethanol, the description of self-assembling and the final structure were still valid. The difference in the ethanol content affected the arrangement of PLs, which tended to migrate in the inner pools of LNPs when ethanol was added to the system. The decrease of PLs on the surface of the nanoparticles could decrease its ability to regulate the particle aggregation, leading to the formation of larger particles when particles are synthesised at lower FRRs. Moreover, higher quantity of ethanol in the system decreased the polarity of the solution, making the lipids less forced to assemble. Consequently, LNPs had a less regular and less compact structure that results in particles of bigger size. These two considerations could motivate the experimental evidence of larger particles produced at lower FRRs.

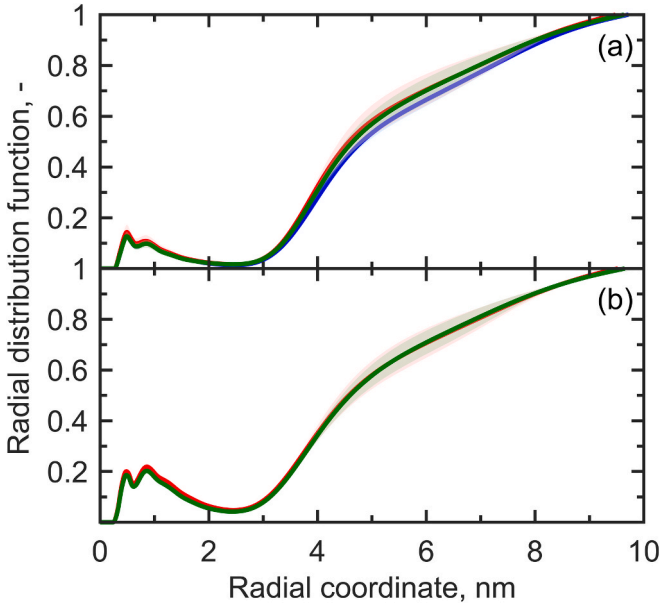

Fig. 7. Radial distribution functions of water (a) and ethanol beads (b) around mRNA in case of FRR equal to (blue curve) 1:0, (green curve) 3:1, and (red curve) 1:1. The solid line represents the average value, while the lighter shade represent the standard deviation over the three replicas of each system. The increase in the ethanol content slightly increased the quantity of solvent in the nanoparticles probably due to an increase in the permeability of the lipidic phase.

The analysis of the affinity of RNA with ILs suggested that Coulombic interactions are not the predominant ones. Despite the Coulombic attraction between the positive charged choline group and the negative charged RNA BB, the head of ILs interacted with the SC in a similar way. Moreover, both the hydroxyl and the ester linker group showed a good affinity with the SC, probably due to the formation of hydrogen bonds. These alternative mechanisms of interactions could explain the affinity

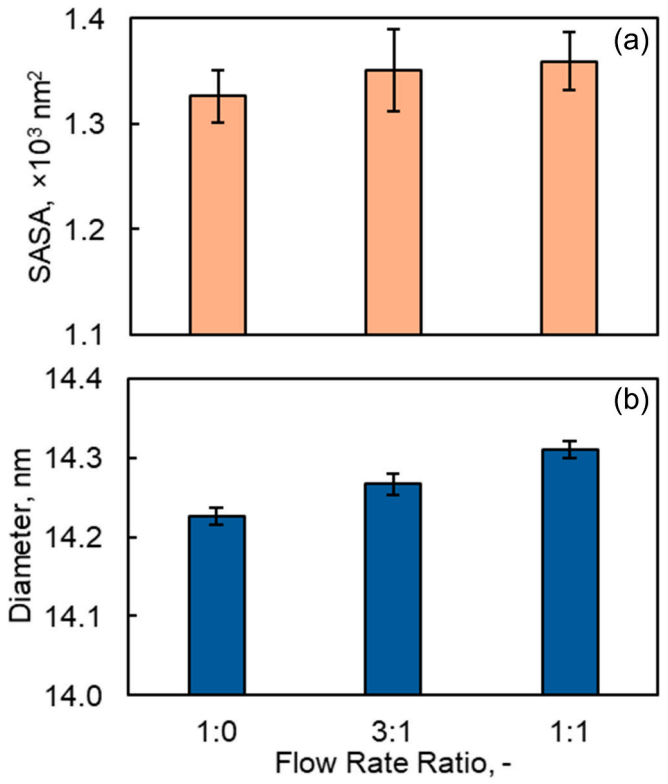

Fig. 8. Solvent accessible surface area (a) and particle size (b) of LNPs as a function of the ethanol molar fraction. The bar represents the average value over the three replicas of the systems, while the error bar represents the standard deviation. Both increased as the molar fraction increased due to the higher solubility of lipids that assemble in a more disordered and less compact structure.

of RNA and ILs even when they are in their neutral form. However, this aspect can be better analysed in future studies by complementing CG simulations with all-atom ones.

These results give a complete overview of the interactions that occur during the synthesis of mRNA-LNP complexes, highlighting the preferential interaction between RNA and the ILs and the effect of the ethanol content on the final assembly. Since CG-MD simulates the system in static conditions, these results could also be extended to other preparations techniques such as bulk mixing. Some differences may be observed due to the different ratios between the aqueous and the organic solvent, but the overall dynamics of the system and the interactions involved would remain unchanged. A precise knowledge of these phenomena could be beneficial in the design of the next generation of lipids for RNA delivery, improving its encapsulation and its stability inside LNPs. This in silico approach could then be extended to any kind of API, optimising the lipidic formulation and the operating conditions for a successful delivery inside human cells.

CRediT authorship contribution statement

Vincenzo Massotti: Writing – original draft, Investigation, Formal analysis, Data curation, Conceptualization. **Antonio Buffo:** Writing – review & editing, Supervision, Resources, Project administration, Methodology, Investigation, Funding acquisition, Data curation, Conceptualization. **Roberto Pisano:** Writing – review & editing, Supervision, Resources, Project administration, Methodology, Investigation, Funding acquisition, Data curation, Conceptualization.

Declaration of competing interest

The authors declare that they have no known competing financial interests or personal relationships that could have appeared to influence the work reported in this paper.

Acknowledgments

The authors sincerely thank Francesco De Roma and Dr Fiora Artusio for their valuable support during the final stage of this study, and ISCRA for awarding this project access to the LEONARDO supercomputer, owned by the EuroHPC Joint Undertaking, hosted by CINECA (Italy). Additional computational resources were provided by HPC@POLITO, a project of Academic Computing within the Department of Control and Computer Engineering at the Politecnico di Torino (http://www.hpc.polito.it).

Appendix A. Supplementary data

Supplementary data to this article can be found online at https://doi.org/10.1016/j.ijpharm.2025.126449.

Data availability

Data will be made available on request.

References

Abraham, M.J., Murtola, T., Schulz, R., Páll, S., Smith, J.C., Hess, B., Lindah, E., 2015. Gromacs: High performance molecular simulations through multi-level parallelism from laptops to supercomputers. SoftwareX 1–2, 19–25. https://doi.org/10.1016/j.softx.2015.06.001.

Arteta, M.Y., Kjellman, T., Bartesaghi, S., Wallin, S., Wu, X., Kvist, A.J., Dabkowska, A., Székely, N., Radulescu, A., Bergenholtz, J., Lindfors, L., 2018. Successful reprogramming of cellular protein production through mRNA delivered by functionalized lipid nanoparticles. PNAS 115, E3351–E3360. https://doi.org/10.1073/pnas.1720542115.

Bernetti, M., Bussi, G., 2020. Pressure control using stochastic cell rescaling. J. Chem. Phys. 153. https://doi.org/10.1063/5.0020514.

Borges-Araújo, L., Borges-Araújo, A.C., Ozturk, T.N., Ramirez-Echemendia, D.P., Fábián, B., Carpenter, T.S., Thallmair, S., Barnoud, J., Ingólfsson, H.I., Hummer, G., Tieleman, D.P., Marrink, S.J., Souza, P.C.T., Melo, M.N., 2023. Martini 3 Coarse-Grained Force Field for Cholesterol. J. Chem. Theory Comput. https://doi.org/10.1021/acs.jctc.3c00547.

Brader, M.L., Williams, S.J., Banks, J.M., Hui, W.H., Zhou, Z.H., Jin, L., 2021. Encapsulation state of messenger RNA inside lipid nanoparticles. Biophys. J. 120, 2766–2770. https://doi.org/10.1016/j.bpj.2021.03.012.

Briuglia, M.L., Rotella, C., McFarlane, A., Lamprou, D.A., 2015. Influence of cholesterol on liposome stability and on in vitro drug release. Drug Deliv. Transl. Res. 5, 231–242. https://doi.org/10.1007/s13346-015-0220-8.

Bussi, G., Donadio, D., Parrinello, M., 2007. Canonical sampling through velocity rescaling. J. Chem. Phys. 126. https://doi.org/10.1063/1.2408420.

Cornebise, M., Narayanan, E., Xia, Y., Acosta, E., Ci, L., Koch, H., Milton, J., Sabnis, S., Salerno, T., Benenato, K.E., 2022. Discovery of a Novel Amino Lipid that Improves Lipid Nanoparticle Performance through specific Interactions with mRNA. Adv. Funct. Mater. 32. https://doi.org/10.1002/adfm.202106727.

Darden, T., York, D., Pedersen, L., 1993. Particle mesh Ewald: an N·log(N) method for Ewald sums in large systems. J. Chem. Phys. 98, 10089–10092. https://doi.org/10.1063/1.464397.

Eygeris, Y., Gupta, M., Kim, J., Sahay, G., 2022. Chemistry of Lipid Nanoparticles for RNA delivery. Acc. Chem. Res. 55, 2–12. https://doi.org/10.1021/acs.accounts.1c00544.

Eygeris, Y., Patel, S., Jozic, A., Sahay, G., Sahay, G., 2020. Deconvoluting Lipid Nanoparticle Structure for Messenger RNA delivery. Nano Lett. 20, 4543–4549. https://doi.org/10.1021/acs.nanolett.0c01386.

Gao, H., Kan, S., Ye, Z., Feng, Y., Jin, L., Zhang, X., Deng, J., Chan, G., Hu, Y., Wang, Y., Cao, D., Ji, Y., Liang, M., Li, H., Ouyang, D., 2022. Development of in silico methodology for siRNA lipid nanoparticle formulations. Chem. Eng. J. 442. https://doi.org/10.1016/j.cej.2022.136310.

Garaizar, A., Díaz-Oviedo, D., Zablowsky, N., Rissanen, S., Köbberling, J., Sun, J., Steiger, C., Steigemann, P., Mann, F.A., Meier, K., 2024. Toward understanding lipid reorganization in RNA lipid nanoparticles in acidic environments. PNAS 121. https://doi.org/10.1073/pnas.2404555121.

Gote, V., Bolla, P.K., Kommineni, N., Butreddy, A., Nukala, P.K., Palakurthi, S.S., Khan, W., 2023. A Comprehensive Review of mRNA Vaccines. Int. J. Mol. Sci. https://doi.org/10.3390/ijms24032700.

Gruner, S.M., Cullis, P.R., Hope, M.J., Tilcock, C.P.S., 1985. Lipid Polymorphism:The Molecular Basis of Nonbilayer Phases. Annu. Rev. Biophys. Biophys. Chem. 14, 211–238. https://doi.org/10.1146/annurev.bb.14.060185.001235.

Grzetic, D.J., Hamilton, N.B., Shelley, J.C., 2024. Coarse-Grained simulation of mRNA-loaded Lipid Nanoparticle Self-Assembly. Mol. Pharm. 21, 4747–4753. https://doi.org/10.1021/acs.molpharmaceut.4c00216.

Hald Albertsen, C., Kulkarni, J.A., Witzigmann, D., Lind, M., Petersson, K., Simonsen, J. B., 2022. The role of lipid components in lipid nanoparticles for vaccines and gene therapy. Adv. Drug Deliv. Rev. https://doi.org/10.1016/j.addr.2022.114416.

Hardianto, A., Muscifa, Z.S., Widayat, W., Yusuf, M., Subroto, T., 2023. The effect of Ethanol on Lipid Nanoparticle Stabilization from a Molecular Dynamics simulation Perspective. Molecules 28. https://doi.org/10.3390/molecules28124836.

Humphrey, W., Dalke, A., Schulten, K., 1996. VMD: Visual Molecular Dynamics.

Israelachvili, J.N., 2011. Intermolecular and Surface Forces. Elsevier Science & Technology, United States.

Kim, J., Eygeris, Y., Gupta, M., Sahay, G., 2021. Self-assembled mRNA vaccines. Adv. Drug Deliv. Rev. https://doi.org/10.1016/j.addr.2020.12.014.

Kjølbye, L.R., VALÉRIO, M., PALONCÝOVÁ, M., BORGES-ARAÚJO, L., PESTANA-NOBLES, R., GRÜNEWALD, F., M. H. BRUININKS, B., ARAYA-OSORIO, R., ŠREJBER, M., MERA-ADASME, R., MONTICELL, L., J. MARRINK, S., OTYEPKA, M., WU, S., C. T. SOUZA, P., 2024. Martini 3 building blocks for Lipid Nanoparticle design. Doi: 10.26434/chemrxiv-2024-bf4n8.

Leung, A.K.K., Hafez, I.M., Baoukina, S., Belliveau, N.M., Zhigaltsev, I.V., Afshinmanesh, E., Tieleman, D.P., Hansen, C.L., Hope, M.J., Cullis, P.R., 2012. Lipid nanoparticles containing siRNA synthesized by microfluidic mixing exhibit an electron-dense nanostructured core. J. Phys. Chem. C 116, 18440–18450. https://doi.org/10.1021/jp303267y.

Market Research Future, https://www.marketresearchfuture.com/reports/mrna-therapeutics-market-10389, Accessed 11 May 2025.

Osouli-Bostanabad, K., Puliga, S., Serrano, D.R., Bucchi, A., Halbert, G., Lalatsa, A., 2022. Microfluidic Manufacture of Lipid-based Nanomedicines. Pharmaceutics. https://doi.org/10.3390/pharmaceutics14091940.

Paloncýová, M., Čechová, P., Šrejber, M., Kührová, P., Otyepka, M., 2021. Role of Ionizable Lipids in SARS-CoV-2 Vaccines As Revealed by Molecular Dynamics Simulations: from Membrane Structure to Interaction with mRNA Fragments. J. Phys. Chem. Lett. 12, 11199–11205. https://doi.org/10.1021/acs.jpclett.1c03109.

Paloncýová, M., Šrejber, M., Čechová, P., Kührová, P., Zaoral, F., Otyepka, M., 2023. Atomistic Insights into Organization of RNA-Loaded Lipid Nanoparticles. J. Phys. Chem. B 127, 1158–1166. https://doi.org/10.1021/acs.jpcb.2c07671.

Paloncýová, M., Valério, M., Dos Santos, R.N., Kührová, P., Šrejber, M., Čechová, P., Dobchev, D.A., Balsubramani, A., Banáš, P., Agarwal, V., Souza, P.C.T., Otyepka, M., 2025. Computational Methods for Modeling Lipid-Mediated active Pharmaceutical Ingredient delivery. Mol. Pharm. https://doi.org/10.1021/acs.molpharmaceut.4c00744.

Pardi, N., Hogan, M.J., Porter, F.W., Weissman, D., 2018. mRNA vaccines-a new era in vaccinology. Nat. Rev. Drug Discov. https://doi.org/10.1038/nrd.2017.243.

Ripoll, M., Martin, E., Enot, M., Robbe, O., Rapisarda, C., Nicolai, M.C., Deliot, A., Tabeling, P., Authelin, J.R., Nakach, M., Wils, P., 2022. Optimal self-assembly of lipid nanoparticles (LNP) in a ring micromixer. Sci. Rep. 12. https://doi.org/10.1038/s41598-022-13112-5.

Rissanou, A.N., Ouranidis, A., Karatasos, K., 2020. Complexation of single stranded RNA with an ionizable lipid: an all-atom molecular dynamics simulation study. Soft Matter 16, 6993–7005. https://doi.org/10.1039/d0sm00736f.

Roces, C.B., Lou, G., Jain, N., Abraham, S., Thomas, A., Halbert, G.W., Perrie, Y., 2020. Manufacturing considerations for the development of lipid nanoparticles using microfluidics. Pharmaceutics 12, 1–19. https://doi.org/10.3390/pharmaceutics12111095.

Rozmanov, D., Baoukina, S., Tieleman, D.P., 2014. Density based visualization for molecular simulation. Faraday Discuss. 169, 225–243. https://doi.org/10.1039/c3fd00124e.

Schoenmaker, L., Witzigmann, D., Kulkarni, J.A., Verbeke, R., Kersten, G., Jiskoot, W., Crommelin, D.J.A., 2021. mRNA-lipid nanoparticle COVID-19 vaccines: Structure and stability. Int. J. Pharm. https://doi.org/10.1016/j.ijpharm.2021.120586.

Shepherd, S.J., Issadore, D., Mitchell, M.J., 2021. Microfluidic formulation of nanoparticles for biomedical applications. Biomaterials. https://doi.org/10.1016/j.biomaterials.2021.120826.

Souza, P.C.T., Alessandri, R., Barnoud, J., Thallmair, S., Faustino, I., Grünewald, F., Patmanidis, I., Abdizadeh, H., Bruininks, B.M.H., Wassenaar, T.A., Kroon, P.C., Melcr, J., Nieto, V., Corradi, V., Khan, H.M., Domański, J., Javanainen, M., Martinez-Seara, H., Reuter, N., Best, R.B., Vattulainen, I., Monticelli, L., Periole, X., Tieleman, D.P., de Vries, A.H., Marrink, S.J., 2021. Martini 3: a general purpose force field for coarse-grained molecular dynamics. Nat. Methods 18, 382–388. https://doi.org/10.1038/s41592-021-01098-3.

Szebeni, J., Kiss, B., Bozó, T., Turjeman, K., Levi-Kalisman, Y., Barenholz, Y., Kellermayer, M., 2023. Insights into the Structure of Comirnaty Covid-19 Vaccine: a Theory on Soft, Partially Bilayer-Covered Nanoparticles with Hydrogen Bond-Stabilized mRNA-lipid Complexes. ACS Nano 17, 13147–13157. https://doi.org/10.1021/acsnano.2c11904.

Trollmann, M.F.W., Böckmann, R.A., 2022. mRNA lipid nanoparticle phase transition. Biophys. J . 121, 3927–3939. https://doi.org/10.1016/j.bpj.2022.08.037.

Ueda, K., Sakagawa, Y., Saito, T., Fujimoto, T., Nakamura, M., Sakuma, F., Kaneko, S., Tokumoto, T., Nishimura, K., Takeda, J., Arai, Y., Yamamoto, K., Ikeda, Y., Higashi, K., Moribe, K., 2023. Molecular-Level Structural Analysis of siRNA-loaded Lipid Nanoparticles by 1H NMR Relaxometry: Impact of Lipid Composition on their Structural Properties. Mol. Pharm. 20, 4729–4742. https://doi.org/10.1021/acs.molpharmaceut.3c00477.

Verbeke, R., Lentacker, I., De Smedt, S.C., Dewitte, H., 2019. Three decades of messenger RNA vaccine development. Nano Today. https://doi.org/10.1016/j.nantod.2019.100766.

Viger-Gravel, J., Schantz, A., Pinon, A.C., Rossini, A.J., Schantz, S., Emsley, L., 2018. Structure of Lipid Nanoparticles Containing siRNA or mRNA by Dynamic Nuclear Polarization-Enhanced NMR Spectroscopy. J. Phys. Chem. B 122, 2073–2081. https://doi.org/10.1021/acs.jpcb.7b10795.

Wang, M.M., Wappelhorst, C.N., Jensen, E.L., Chi, Y.C.T., Rouse, J.C., Zou, Q., 2023. Elucidation of lipid nanoparticle surface structure in mRNA vaccines. Sci. Rep. 13. https://doi.org/10.1038/s41598-023-43898-x.

Wang, R., Zhang, Y., Zhong, H., Zang, J., Wang, W., Cheng, H., Chen, Y., Ouyang, D., 2025. Understanding the self-assembly and molecular structure of mRNA lipid nanoparticles at real size: Insights from the ultra-large-scale simulation. Int. J. Pharm. 670. https://doi.org/10.1016/j.ijpharm.2024.125114.

Xu, L., Wang, X., Liu, Y., Yang, G., Falconer, R.J., Zhao, C.X., 2022. Lipid Nanoparticles for Drug delivery. Adv. NanoBiomed Res. https://doi.org/10.1002/anbr.202100109.

Zhang, Z., Cheng, D., Luo, W., Hu, D., Yang, T., Hu, K., Liang, L., Liu, W., Hu, J., 2024. Molecular Dynamics simulation of Lipid Nanoparticles Encapsulating mRNA. Molecules 29. https://doi.org/10.3390/molecules29184409.